

1 **Drivers and reversibility of abrupt ocean state**
2 **transitions in the Amundsen Sea, Antarctica**

3 **Justine Caillet¹, Nicolas C. Jourdain¹, Pierre Mathiot¹, Hartmut H. Hellmer²,**
4 **J r mie Mouginot¹**

5 ¹Univ. Grenoble Alpes, CNRS, IRD, Grenoble INP, IGE, 38000 Grenoble, France

6 ²Alfred Wegener Institute Helmholtz Centre for Polar and Marine Research, Bremerhaven, Germany

7 **Key Points:**

- 8 • The currently warm ice-shelf cavities of the Amundsen sector could become or have
9 been cold for slightly colder climatic conditions.
10 • The transitions are reversible:cancelling the atmospheric perturbation brings the
11 ocean back to its unperturbed state within a few decades.
12 • All the transitions are primarily driven, at multi-decadal scale, by changes in sur-
13 face buoyancy fluxes over the continental shelf.

Corresponding author: Justine CAILLET, justine.caillet@univ-grenoble-alpes.fr

Abstract

Ocean warming around Antarctica has the potential to trigger marine ice-sheet instabilities. It has been suggested that abrupt and irreversible cold-to-warm ocean tipping points may exist, with possible domino effect from ocean to ice-sheet tipping points. A $1/4^\circ$ ocean model configuration of the Amundsen Sea sector is used to investigate the existence of ocean tipping points, their drivers, and their potential impact on ice-shelf basal melting. We apply idealized atmospheric perturbations of either heat, freshwater or momentum fluxes, and we characterize the key physical processes at play in warm-to-cold and cold-to-warm climate transitions. Relatively weak perturbations of any of these fluxes are able to switch the Amundsen Sea to an intermittent or permanent cold state, i.e., with ocean temperatures close to the surface freezing point and very low ice-shelf melt rate. The transitions are reversible, i.e., cancelling the atmospheric perturbation brings the ocean system back to its unperturbed state within a few decades. All the transitions are primarily driven by changes in surface buoyancy fluxes over the continental shelf, as a direct consequence of the freshwater flux perturbation, or through changes in net sea-ice production resulting from either heat flux perturbations or from changes in sea-ice advection for the momentum flux perturbation. These changes affect the vertical ocean stratification and thereby ice-shelf basal melting. For warmer climate conditions than presently, the surface buoyancy forcing becomes less important as there is a decoupling between the surface and subsurface layers, and ice-shelf melt rates appear less sensitive to climate conditions.

Plain Language Summary

The West Antarctic Ice Sheet is under the threat of a partial collapse, which would induce rapid global sea level rise. This threat is partly related to the thinning of floating ice shelves, and the consequent retreat of the grounding line, which is a self-sustained ice dynamics process. It is triggered by increased basal melting of the ice shelves, which results from enhanced flow of relatively warm waters onto the continental shelf. It has been suggested that self-sustained ocean processes may lead to abrupt changes in the flow of warm water into ice-shelf cavities, which could facilitate the tipping to a marine ice-sheet instability. Here, we analyze whether such abrupt ocean changes can occur under cold-to-warm or warm-to-cold transitions in the Amundsen Sea, West Antarctica. We use a regional ocean model with a set of idealized local atmospheric perturbations to characterize the thresholds and reversibility of ocean abrupt changes. We find that the currently warm Amundsen Sea could switch intermittently or permanently to a cold state for relatively weak atmospheric perturbations and could be slightly warmer in the future. All transitions are reversible. The main mechanism involved on decadal scale is related to a change in the surface buoyancy fluxes.

1 Introduction

The West Antarctic Ice Sheet has lost mass over the last few decades and has thus contributed significantly to global sea level rise. Warming of the oceanic sub-surface seems to have caused an increase in melting under floating ice shelves, particularly in the Amundsen Sea (Jenkins et al., 2018). Depending on the bedrock slope direction (Schoof, 2007; Pattyn et al., 2012) and ice-shelf lateral buttressing (Gudmundsson, 2013), a sufficiently strong and persistent increase in basal melting can lead to a Marine Ice-Sheet Instability (MISI), resulting in a self-sustained retreat of the glacier’s grounding line and to the acceleration of its flow (Favier et al., 2014; Joughin et al., 2014).

Instabilities are triggered above a certain oceanic warming (critical threshold or tipping point), with the possible existence of multiple thresholds. Thus, Rosier et al. (2021) estimated that Pine Island Glacier would undergo a MISI and major mass loss for an oceanic warming of $+1.2^\circ\text{C}$ relative to the present. Garbe et al. (2020) estimated that

64 a tipping point of +2°C global warming relative to pre-industrial could cause a MISI of
 65 the entire West Antarctic Ice Sheet. Tipping points are characterized by a hysteresis,
 66 i.e., restoring the forcing to before the occurrence of the tipping point is not sufficient
 67 to restore the system to its original state. Identifying these tipping points precisely and
 68 linking them to climate projections would allow the effects of future rapid sea level rise
 69 to be anticipated and possibly mitigated (Hinkel et al., 2019).

70 The abrupt nature of these ice tipping points in West Antarctica could be enhanced
 71 if ocean warming itself is subject to a tipping point. This would be a cascading tipping
 72 point, or domino effect (Dekker et al., 2018; Brovkin et al., 2021; Wunderling et al., 2021).
 73 It has been suggested, that beyond a certain threshold of melting, the Greenland Ice Sheet
 74 could induce a sudden weakening of the Atlantic Meridional Overturning Circulation,
 75 which, in turn, would lead to ocean warming around Antarctica (Turney et al., 2020; Wun-
 76 derling et al., 2021).

77 Another type of oceanic tipping point has been highlighted in the Weddell Sea (Hellmer
 78 et al., 2012, 2017). Reduced sea-ice formation under continued global warming, a fresh-
 79 ening of the continental shelf, and increased ocean surface stress could cause the slope
 80 current to diverge in the southeast Weddell Sea. The reorientation would facilitate the
 81 entry of Warm Deep Water, a cooler variant of Circumpolar Deep Water (CDW), onto
 82 the continental shelf and significantly increase basal melting, which would lead to a self-
 83 reinforcing process due to the injection of meltwater. The process is irreversible with the
 84 twentieth-century atmospheric forcing: only an imposed decrease in basal melt rate can
 85 hinder the self-sustaining process.

86 The Amundsen Sea environment is very different as relatively warm cavities already
 87 exist (Jacobs et al., 1996, 2012). Paleoclimatic indicators suggest that the entire Amund-
 88 sen continental shelf was covered by an ice sheet (either resting or floating) at the Last
 89 Glacial Maximum (Larter et al., 2014). A particularly large retreat of the ice-sheet front
 90 and grounding line occurred between 20,000 and 10,000 years BP (Larter et al., 2014),
 91 with further smaller retreats occurring thereafter, notably around 1945 and then 1970
 92 (Smith et al., 2017). Ocean temperatures and warming rates during these transitions are
 93 not known, but it is possible that oceanic tipping points similar to those reported by Hellmer
 94 et al. (2012, 2017) for the Weddell Sea occurred in the Amundsen Sea area as well.

95 In this paper, we analyze under which atmospheric forcing conditions warm-to-cold,
 96 cold-to-warm and warm-to-warmer ocean transitions in the Amundsen Sea have occurred
 97 or could occur, and we test the reversibility of these transitions, i.e., the presence of hys-
 98 teresis. We use a regional ocean modelling approach with a set of idealized atmospheric
 99 perturbations.

100 2 Materials and Methods

101 2.1 Model and configuration

102 The Nucleus for European Modelling of the Ocean (NEMO) model, version 3.6, in-
 103 cluding the OPA ocean model (Madec & the NEMO Team, 2016) and the Louvain-la-
 104 Neuve sea-ice model LIM-3.6 (Rousset et al., 2015), is used in a regional configuration
 105 of the Amundsen Sea (Fig. 1). Our model parameters are similar to Jourdain et al. (2019),
 106 with a representation of ice–ocean exchange beneath static ice shelves, with melt rate
 107 depending on ocean velocity, temperature and salinity (Mathiot et al., 2017; Jourdain
 108 et al., 2017), and barotropic tides prescribed as lateral boundary conditions from seven
 109 constituents of the FES2012 tidal model (Carrère et al., 2012; Lyard et al., 2006).

110 Compared to Jourdain et al. (2019), the domain is slightly extended, now cover-
 111 ing from 142°W to 85°W and from 76.3°S to 59.8°S, and the resolution is reduced to 1/4°
 112 in longitude, i.e., a quasi-isotropic resolution ranging from 14 km at the northern bound-

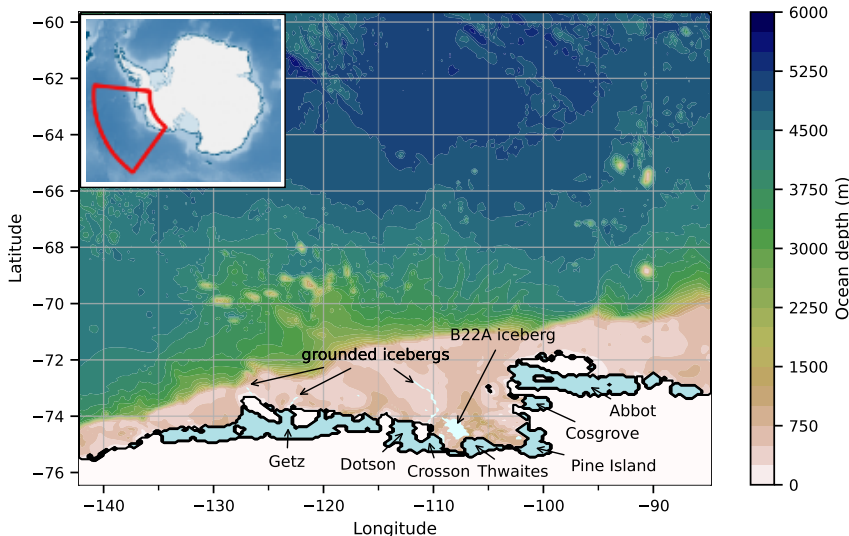


Figure 1. Used regional configuration of the Amundsen Sea. Bathymetry and ice-shelf draft are from the second version of the BedMachine Antarctica dataset (Morlighem et al., 2020). Grounded ice is shaded in white, ice shelves are colored in blue and main tabular icebergs in light cyan. The general view is drawn from the geospatial data package Quantarctica (Matsuoka et al., 2021).

113 ary to 6.5 km in the southernmost part of the domain. Bathymetry, as well as surface
 114 and lateral boundary conditions also differ from Jourdain et al. (2019) and cover the pe-
 115 riod 1958-2018 in this study. The period 1958-1968 is left for spin-up and discarded in
 116 our analyses.

117 The bathymetry and ice-shelf draft interpolated on the model grid are from the sec-
 118 ond version of the BedMachine Antarctica dataset (Morlighem et al., 2020). This recent
 119 dataset represents Thwaites Ice Shelf after its partial collapse. The B22A iceberg as well
 120 as other very large tabular icebergs, absent from BedMachine Antarctica, are represented
 121 as static flat ice shelves in the middle of the ocean (assumed to be grounded by the subgrid-
 122 scale bathymetry when no grounded area is explicitly represented). Their shape and
 123 location are derived from a MODIS-visible image (provided by the US National Snow
 124 and Ice Data Center) taken on 5th September 2003. The huge B22A iceberg calved from
 125 the Thwaites ice tongue in 2002 and has drifted very slowly since then (Antarctic Ice-
 126 berg Tracking Database, Budge & Long, 2018). A similar calving event occurred in the
 127 late 1960s (Lindsey, 1995). The resulting iceberg was eventually designated B10 in 1992
 128 when it started a 15-year drift across the Amundsen Sea before breaking up and drift-
 129 ing further away (Budge & Long, 2018). Numerous smaller icebergs regularly drift west-
 130 ward in the Amundsen Sea and ground on the eastern flank of bathymetric ridges shall-
 131 er than approximately 400 m (Mazur et al., 2017). We therefore artificially place a
 132 wall along the 380 m isobath on the eastern flank of Bear Ridge (in a similar way as Bett
 133 et al., 2020), north of Siple Island, and on the main ridge in between. These permanent
 134 lines of grounded icebergs were shown to favor the formation of polynyas with impact
 135 on ice-shelf melting (Nakayama et al., 2014; Bett et al., 2020).

136 The conditions at the lateral ocean and sea-ice boundaries are derived from the 5-
 137 day mean outputs of a global simulation very similar to the one described in Merino et
 138 al. (2018) except that it is spun up from 1958 and that the imposed ice-shelf melt flux
 139 increases linearly from 1990 to 2005 and is constant before and after that, with values

140 corresponding to the FRESH+ and FRESH– reconstructions of Merino et al. (2018).
 141 Here, the temperature and salinity boundary conditions are corrected by the difference
 142 between the seasonal climatology of the World Ocean Atlas 2018 (WOA18) database (Garcia
 143 et al., 2019) and the seasonal climatology of the global simulation. The global simula-
 144 tion used for boundary conditions represents melting of Lagrangian icebergs (Merino et
 145 al., 2016), and the corresponding 5-day mean melt fluxes are applied as a freshwater flux
 146 at the surface of our regional configuration. The atmospheric forcing data are taken from
 147 the JRA55-do reanalysis (Tsujino et al., 2018) between 1958 and 2018. The fluxes be-
 148 tween ocean (or sea ice) and atmosphere are calculated using the CORE bulk formulae
 149 described in Griffies et al. (2009); Large and Yeager (2004).

150 Some model parameters are varied to reduce biases in the reference configuration
 151 (see Supporting Information), while atmospheric forcing fields are perturbed (Section 2.2)
 152 to investigate ocean tipping points.

153 2.2 Atmospheric forcing perturbations

154 In the following, we investigate three pathways to induce ocean tipping points in
 155 the Amundsen Sea through surface flux modifications of either heat, freshwater, or mo-
 156 mentum. We decided to consider idealized atmospheric perturbations in order to iden-
 157 tify and isolate the processes at play. Thus, each surface flux is perturbed independently.

158 The heat flux is perturbed through air temperature, to which the flux is particu-
 159 larly sensitive. To limit the impact of this perturbation on evaporation, and thus on the
 160 freshwater flux, specific humidity is also modified consistently with the air temperature
 161 perturbation, according to the Clausius Clapeyron law. The choice of air temperature
 162 is convenient for the definition of the perturbation range, which is bounded by typical
 163 conditions of the Last Glacial Maximum, i.e., approximately -10°C relative to the cur-
 164 rent temperature (Masson-Delmotte et al., 2010) and by typical projections at 2300 un-
 165 der the SSP5-8.5 scenario, i.e., about 10°C warmer than the current situation (Lee et al.,
 166 2021).

167 For the freshwater flux, we decide to modify precipitation while maintaining the
 168 ratio between solid and liquid precipitation for the sake of simplicity (the heat flux as-
 169 sociated with snow melting in the ocean is relatively low). Precipitation near Antarc-
 170 tica has been shown to evolve following the Clausius-Clapeyron law (Ligtenberg et al.,
 171 2013; Donat-Magnin et al., 2021). The range of variation is therefore indexed to the tem-
 172 perature range considered for the heat flux: precipitation is multiplied by factors between
 173 0.48 and 1.99, corresponding to coldest (-10°C) and warmest ($+10^{\circ}\text{C}$) climatic conditions,
 174 respectively.

175 The momentum flux is perturbed through meridional shifting of winds. To main-
 176 tain flux independence, only the wind involved in the momentum flux calculation (i.e.,
 177 ocean and sea ice surface friction) is modified, while we keep the wind seen by latent and
 178 sensible heat fluxes unchanged in the bulk formulae. The applied wind shift ranges be-
 179 tween a 4.7° northward shift for coldest (-10°C) climatic conditions (Gray et al., 2021)
 180 and a 4.7° southward shift for warmest ($+10^{\circ}\text{C}$) conditions (extrapolated from the 2100
 181 CMIP5-RCP8.5 sensitivity described in Spence et al., 2014).

182 For the three types of perturbations, we conduct simulations with intermediate per-
 183 turbations between the coldest and warmest climate perturbations in order to better char-
 184 acterize potential tipping points. Perturbations are local, only applied on continental shelf
 185 and slope. We do not perturb lateral boundary conditions, i.e., we maintain the pres-
 186 ence of CDW in front of the continental shelf in all our simulations. It seems clear that
 187 cold conditions would prevail if CDW stopped to exist, and it is more interesting to iden-
 188 tify how warm-to-cold abrupt transitions could occur in the presence of CDW.

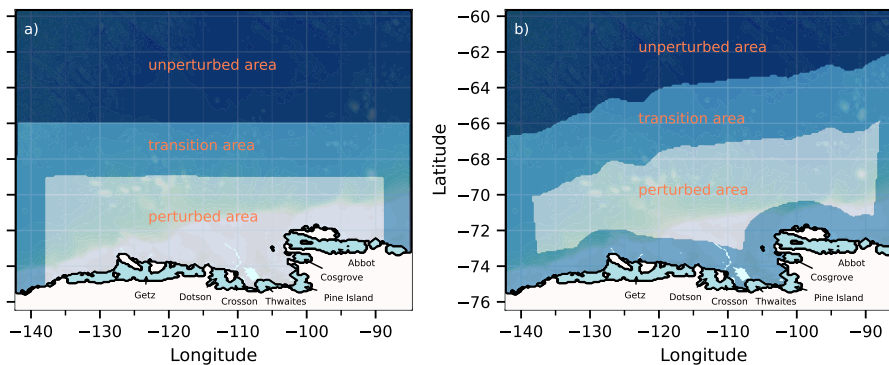


Figure 2. Location of the perturbed area (a) for heat and freshwater fluxes and (b) for momentum flux. The perturbed area is highlighted in light blue, the transition area in blue and the unperturbed area in dark blue. The transition area avoids the artificial formation of strong density gradient or wind curl.

189 Basal melting highly depends on whether the perturbation is applied only on the
 190 continental shelf or on the continental shelf and slope (not shown). We decided to in-
 191 clude the continental slope in the perturbed area as this area is relevant for CDW in-
 192 truding onto the shelf. The ice shelf melt rates are not sensitive to further northward
 193 extension of the perturbation area, which indicates some robustness of our methodol-
 194 ogy. For the heat and freshwater flux perturbations, a transition area of 3° in latitude
 195 (about 340 km) and 4° in longitude limits the temperature and precipitation gradient,
 196 and thus the formation of strong density gradients, between the perturbed and unper-
 197 turbed areas (Fig. 2a). For the momentum flux perturbation, we additionally put a coastal
 198 transition area of 150 km width between the perturbed wind and the katabatic winds
 199 near the ice-sheet edges to avoid creating a substantial artificial wind curl perturbation
 200 (Fig. 2b).

201 2.3 Simulations

202 In order to assess the model response to atmospheric perturbations, we run a 61-
 203 year simulation over the period 1958-2018. The simulation length is a compromise be-
 204 tween computational cost and the description of the natural decadal variability of the
 205 ocean system, which can potentially impact the system stability and the occurrence of
 206 tipping points. The reference experiment corresponds to the configuration retained af-
 207 ter calibration (see Supporting Information) with natural atmospheric and oceanic forc-
 208 ing over the modelled period. The model calibration improves the fidelity of the refer-
 209 ence simulation although the interannual variability is smaller than expected (consequences
 210 will be discussed in section 4). The model spin-up is achieved after 10 years, thus, only
 211 the period 1968-2018 is analyzed. The perturbed runs are identical to the reference run
 212 except for the atmospheric forcing. We study three possible types of transition: cold-
 213 to-warm transitions as reported by Hellmer et al. (2012, 2017) for the Weddell Sea, warm-
 214 to-cold and warm-to-warmer transitions related to ancient or distant future climate tran-
 215 sitions. When an abrupt ocean transition occurs, reversibility is studied, i.e., for cold-
 216 to-warm (C2 in Fig. 3) and warm-to-cold transitions (C3 in Fig. 3).

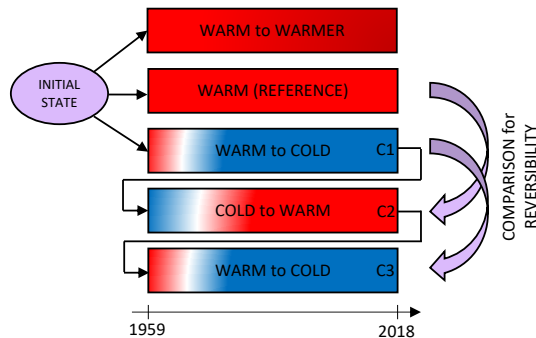


Figure 3. Simulation set-up. The annotations C1, C2 and C3 correspond to the 1st, 2nd and 3rd simulation cycle, respectively. The warm-to-warmer, warm-to-cold (C1) and cold-to-warm simulations enable us to identify the possible existence of transitions and the atmospheric conditions under which they occur. The cold-to-warm (C2) and warm-to-cold (C3) simulations are used to study their reversibility.

3 Results

3.1 Description of the transitions and their reversibility

For the sake of clarity, this section focuses on the mean melt rate of Pine Island and Thwaites on the one hand, and of Crosson and Dotson ice shelves on the other hand. Cosgrove and Getz ice shelves undergo similar melt transitions, albeit with much lower and higher mean melt values, respectively (not shown).

For Pine Island–Thwaites, the heat flux perturbations lead to a permanent collapse of ice-shelf melting for air cooled by 2.5°C or more, with average melt rates below 0.3 m.w.e.yr⁻¹ (meters of water equivalent per year, i.e., 1 m.w.e.yr⁻¹ = 1000 kg.m².yr⁻¹), comparable to those experienced by the Ronne or Eastern Ross ice shelves (Rignot et al., 2013) (Fig. 4a). The -1°C perturbation leads to a collapse of melt rates after year 2000, while the -0.5°C perturbation keeps relatively high melt rates. Cycling our simulations by repeating the period 1958–2018 indicates that the cooler state over 2000–2018 is related to the forcing data and not to a slow drift of our regional system as melt rates are again high before 2000 in the repeated simulations (not shown). The heat flux perturbations associated with higher air temperatures lead to a limited increase in basal melt rates, with no more than a 34% increase for the +10°C perturbation. The effect of increasing air temperatures seems to saturate, with little differences between +2°C and +10°C warming. Basal melt rates beneath Crosson–Dotson show a similar behavior as Pine Island–Thwaites, with intermittent periods of very low melt rates for perturbations as small as -0.5°C, permanent collapse of melt rates below -2.5°C (melt rate is slightly higher than that of Pine Island–Thwaites with typical values of 0.8–1.0 m.w.e.yr⁻¹), and a 28% increase in melt rates for +10°C (Fig. 5a). It can also be noted that the amplitude of the seasonal melt cycle increases in response to warm perturbations for Pine Island–Thwaites but not for Crosson–Dotson.

The freshwater flux perturbations associated with lower precipitation lead to intermittent reductions in melt rates for precipitation reduced by 30% or more for Pine Island–Thwaites (Fig. 4b). Particularly low melt rates are found in the mid 1970s, early 2000s and late 2010s, but never reach the extremely low values resulting from the heat flux perturbations. This contrasts with Crosson–Dotson for which extended periods of very low melt rates (below 1.1 m.w.e.yr⁻¹) are found when precipitation is reduced by 20% or more (Fig. 5b). Increased precipitation does not have a strong effect on melt rates,

249 with only 17% and 9% increase in response to doubled precipitation for Pine Island–Thwaites
 250 and Crosson–Dotson, respectively.

251 Finally, the momentum flux perturbations associated with northward-shifted wind
 252 at Pine Island–Thwaites results in intermittent decreases in melt rates, which is notice-
 253 able for a 2° northward wind shift (Fig. 4c). An extended collapse of basal melting is found
 254 over the period 2000–2018 for a northward wind shift of 4.7° . The extended period of low
 255 melt rates matches relatively well with those found for reduced precipitation. Crosson–
 256 Dotson is again more sensitive, with extended periods of very low melt rates for north-
 257 ward wind shift by 1° or more (Fig. 5c). The poleward-shifted winds lead to minor changes
 258 in basal melting: less than 5% and 15% increase for Pine Island–Thwaites and Crosson–
 259 Dotson, respectively.

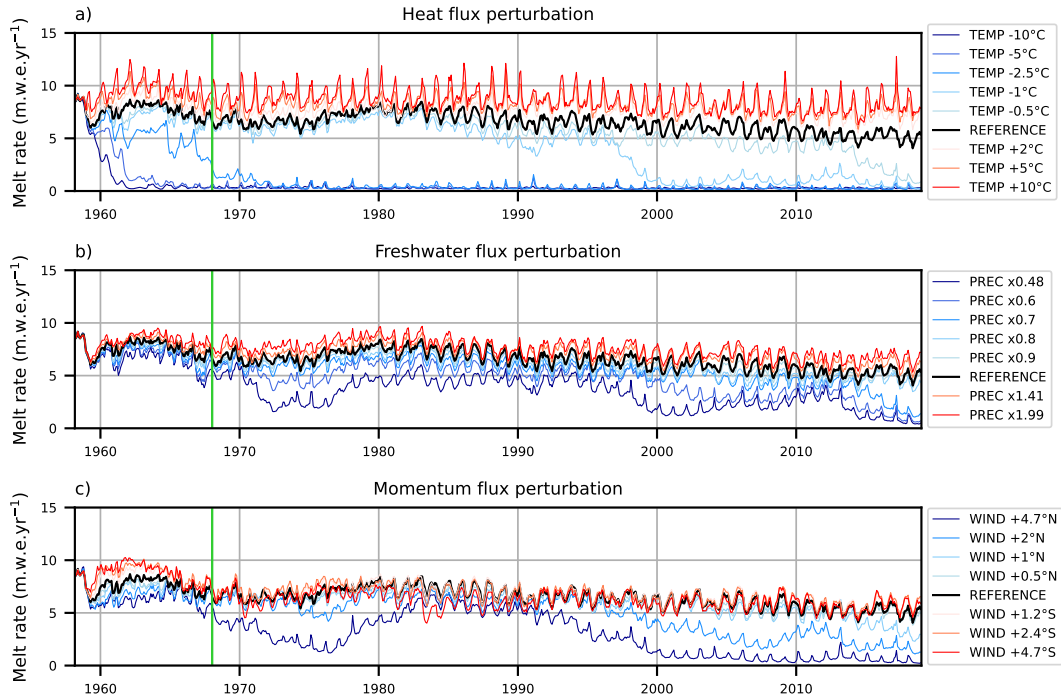


Figure 4. Evolution of monthly basal melting for Pine Island and Thwaites ice shelves over the period 1958–2018 for perturbations of (a) heat flux, (b) freshwater flux, and (c) momentum flux. The black curve (reference curve) corresponds to the simulation with the JRA55 reanalysis without modification. The red and blue curves correspond to simulations with atmospheric perturbations that aim to increase and decrease basal melting, respectively. The vertical green line indicates the end of the 10-year spin up.

260 We have just shown that abrupt transitions from a permanently high to a perma-
 261 nently low melt state can exist, and we now address the reversibility of these warm-to-
 262 cold transitions. We focus on transitions resulting from the strongest perturbations, i.e.,
 263 air cooled by 10°C , precipitation decreased by 52%, and winds shifted northward by 4.7° ,
 264 and we revert the atmospheric forcing to zero perturbation to re-run the period 1958–
 265 2018 starting from the 2018 perturbed state (Fig. 3). After 14 to 21 years, all perturbed
 266 melt time series go back to the unperturbed state and remain within $\pm 5\%$ of the origi-
 267 nal time series (Fig. 6). We conclude that all our warm-to-cold transitions in the Amund-
 268 sen Sea are reversible. This also means that our description of the warm-to-cold transi-
 269 tions can be reverted to describe the cold-to-warm transitions.

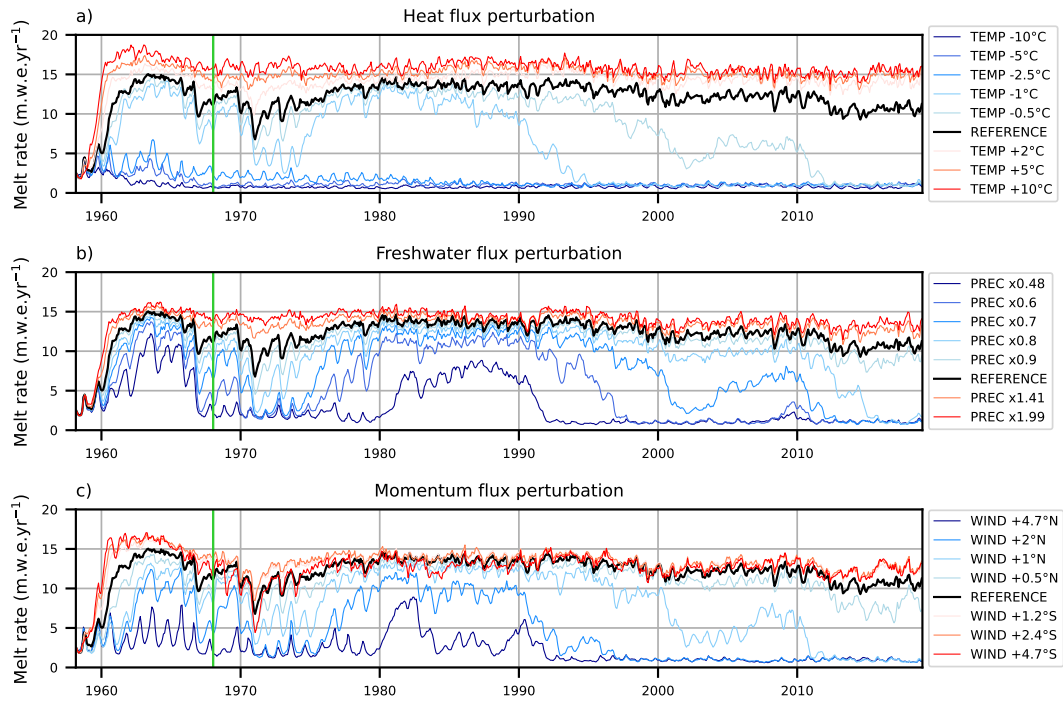


Figure 5. Evolution of monthly basal melting for Crosson and Dotson ice shelves over the period 1958-2018 for perturbations of (a) heat flux, (b) freshwater flux, and (c) momentum flux.. The black curve (reference curve) corresponds to the simulation with the JRA55 reanalysis without modification. The red and blue curves correspond to simulations with atmospheric perturbations that aim to increase and decrease basal melting, respectively. The vertical green line indicates the end of the 10-year spin-up.

270 We also evaluate the reversibility of cold-to-warm transitions, bearing in mind that
 271 such transitions may have occurred in the past. To do this, we take the final state of the
 272 2nd cycle of 1958-2018 (unperturbed warm-climate (natural) forcing following a first cold-
 273 climate perturbed cycle), and we run a 3rd cycle of 1958-2018 again driven by the cold-
 274 climate perturbed forcing (Fig. 3). The two perturbed simulations (1st and 3rd cycle)
 275 converge (within $\pm 5\%$) after 5-6 years for the perturbed heat flux, after 13-20 years for
 276 the perturbed freshwater flux and after 24-34 years for the perturbed momentum flux
 277 (Fig. 7). We conclude that the cold-to-warm transitions are also reversible in the Amund-
 278 sen Sea.

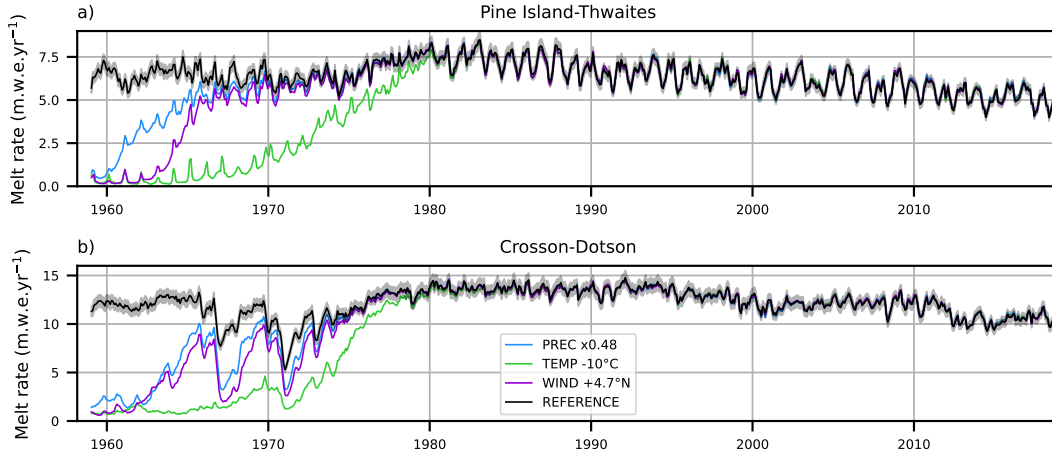


Figure 6. Evolution of the reversed warm-to-cold transition for (a) Pine Island and Thwaites ice shelves and (b) Crosson and Dotson ice shelves. Only the cold-climate perturbations of maximum amplitude are drawn. The black curve corresponds to the simulation driven by the JRA55 reanalysis without modification (natural state), with shading indicating $\pm 5\%$.

279 3.2 Physical processes

280 From a general perspective, the main external drivers of ocean variations are (i)
 281 wind stress changes and (ii) surface heat and freshwater fluxes that modify the sea sur-
 282 face buoyancy (e.g., Marshall & Plumb, 2008; Talley et al., 2011). Winds induce a tan-
 283 gential stress at the ocean surface (directly or via sea-ice advection) and, thus, induce
 284 surface water transport towards the side of the wind. This transport results in areas of
 285 divergence and convergence that lead, respectively, to upwelling (Ekman suction) and
 286 downwelling (Ekman pumping). Surface heat and freshwater fluxes modify the sea sur-
 287 face buoyancy, which can affect convection and the horizontal circulation via density gra-
 288 dents. At high latitudes, the net sea-ice production plays a key role in these processes.

289 Here, we analyze the Ekman vertical velocity (w_{Ek}) and buoyancy flux at the ocean
 290 surface (B_s) to assess the impact of atmospheric forcing perturbations on the ocean prop-
 291 erties. They are defined as:

$$w_{Ek} = \frac{1}{\rho_0} \vec{\nabla}_z \wedge \left(\frac{\vec{\tau}}{f} \right) \quad (1)$$

$$B_s = \frac{g\alpha}{c_p} Q + g\beta S_s F \quad (2)$$

292 where w_{Ek} is the upward Ekman vertical velocity, ρ_0 the reference seawater density, $\vec{\tau}$
 293 the wind/sea-ice stress at the ocean surface and f the Coriolis parameter. B_s is the buoy-
 294 ancy flux at the ocean surface, c_p the specific heat, g the gravitational acceleration, S_s
 295

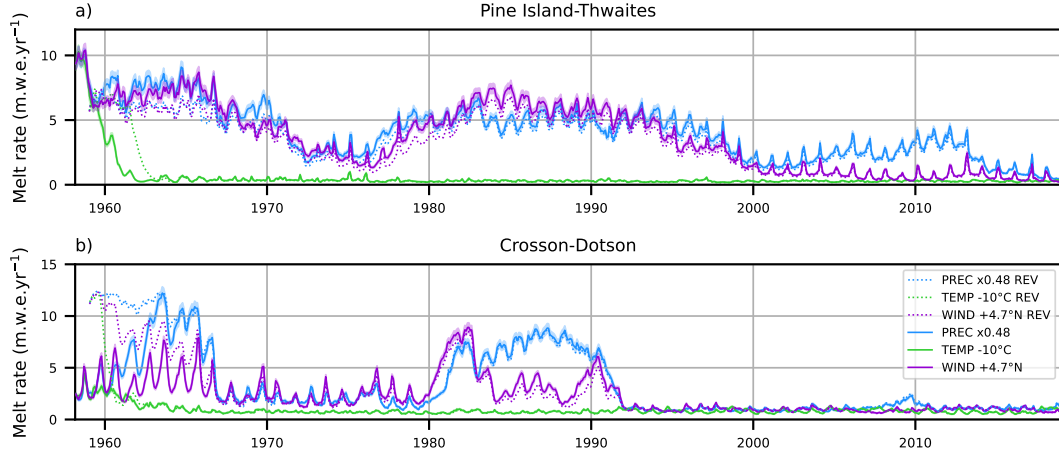


Figure 7. Evolution of the reversed cold-to-warm transition for (a) Pine Island and Thwaites ice shelves and (b) Crosson and Dotson ice shelves. Only the cold -climate perturbations of maximum amplitude are drawn. The solid line represents the melt rate after applying the cold-climate perturbations for the first time over 1958-2018 (1st cycle). The dotted line represents the melt rate under the cold-climate perturbations (3rd cycle) following a 1958-2018 cycle of unperturbed conditions (2nd cycle). The shading corresponds to the melt value of the perturbed state of the 1st cycle $\pm 5\%$.

296 the sea surface salinity, α the surface thermal expansion coefficient of seawater and β the
 297 corresponding coefficient for salinity, F and Q are the heat and freshwater fluxes received
 298 by the ocean surface (positive downward).

299 A striking feature of our ensemble of experiments is that all types of perturbation
 300 approximately have the same ice-shelf melt evolution as a function of the surface buoy-
 301 ancy flux over the continental shelf (Fig. 8). The evolution curve consists of a highly sen-
 302 sitive regime bounded by a low plateau with no melt variations and a high plateau with
 303 lower melt sensitivity. The similarity between the three curves in Fig. 8 suggests that
 304 all perturbations mostly modify melt rates through changes of the surface buoyancy fluxes.
 305 Hereafter, we describe the processes that affect the surface buoyancy for the various types
 306 of perturbations.

307 The freshwater flux perturbations ("PREC" in Fig. 8) are the easiest to understand
 308 as precipitation directly affects the surface buoyancy. Lowering precipitation reduces the
 309 vertical density gradient and thereby favors convective mixing (Fig. 9c), which extracts
 310 the heat of the deep spreading CDW. A much colder water below the thermocline (Fig. 9a)
 311 explains the lower melt rates in the experiments with reduced precipitation. The oppo-
 312 site mechanism explains higher melt rates in the presence of enhanced precipitation. A
 313 small part of the freshwater flux modification is also related to minor changes in sea-ice
 314 production (Fig. 10a), due to the insulating properties of snow on sea ice (not shown).

315 The heat flux perturbations ("TEMP" in Fig. 8) have a less direct effect on sur-
 316 face buoyancy than just thermal expansion. Modified heat fluxes indeed explain less than
 317 25% of the changes in surface buoyancy fluxes, while changes in freshwater fluxes related
 318 to net sea-ice production (i.e., growth minus melt) have a preponderant effect on the sur-
 319 face buoyancy fluxes. In the presence of colder air, the net sea-ice production increases
 320 considerably over the continental shelf (Fig. 10a), mostly due to a drastic decrease in sum-
 321 mer melting (not shown). The case is very similar to decreased precipitation, albeit with
 322 a larger amplitude: increased convective mixing and related cooling below the thermo-

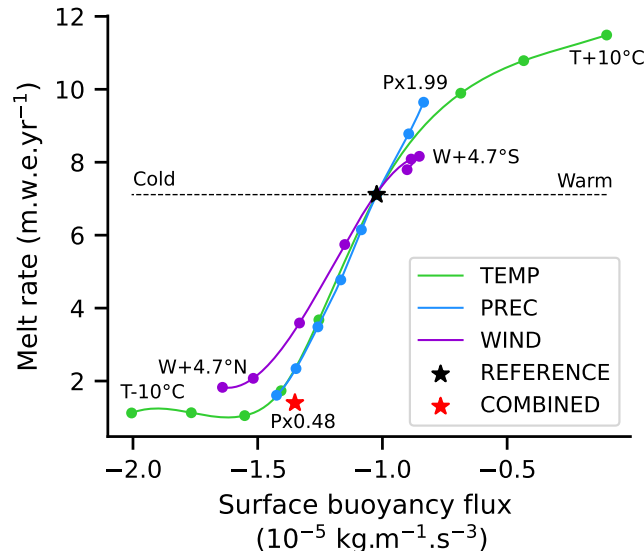


Figure 8. Mean ice-shelf melt rate in the Amundsen Sea as a function of the mean surface buoyancy flux over the Amundsen Sea continental shelf over the period 1988-2018. The green, blue and purple curves correspond to perturbations of heat, freshwater and momentum fluxes, respectively. The black star represents the reference case. The red star represents a more realistic case. It corresponds to the current climate - 0.5°C by combining the perturbation of all the fluxes (TEMP -0.5°C, PREC x0.96 and WIND +0.24°N).

323 cline (Fig. 9d,e,f) leads to reduced ice-shelf melting (Fig. 8). Its minimum is reached when
 324 the entire water column is close to the surface freezing temperature and the ice-shelf cav-
 325 ities are cold, i.e., melt rates are low and only controlled by the pressure dependency of
 326 the freezing point. For the warm perturbations, the opposite effect exists until there is
 327 too little net sea-ice production (Fig. 10a) to induce convective mixing. Beyond that,
 328 the CDW layer remains mostly unchanged and ice-shelf melt rates keep increasing only
 329 because warmer surface water gets in contact with the ice-shelf base (Fig. 9d,e,f). This
 330 is consistent with the aforementioned increased seasonality of the Pine Island and Thwaites
 331 melt rates (Fig. 4).

332 The results of the momentum flux perturbations are probably the most surprising
 333 as they affect the surface buoyancy fluxes (see "WIND" in Fig. 8), although we have been
 334 cautious not to modify the wind field in the calculation of the turbulent heat and evap-
 335 oration fluxes. The impact of winds on sea-ice drift actually explains the variation in buoy-
 336 ancy flux. In the experiments with a northward wind shift, the net production increases
 337 (Fig. 10a) as winter sea-ice growth increases and summer melting decreases (not shown),
 338 but the sea-ice volume decreases (frozen area and thickness decrease in Fig. 10b,c). This
 339 is explained by enhanced advection of thinner sea ice towards the deep ocean (Fig. 11),
 340 which leaves space for more air-sea exchange on the continental shelf, i.e., more sea-ice
 341 production. Therefore, it is a similar perturbation of the vertical ocean stratification as
 342 in the case of the freshwater and heat perturbations. In the case of a southward wind
 343 shift, the annual sea-ice characteristics are little changed (Fig. 10) and so is the mean
 344 ice-shelf melt rate (Fig. 8).

345 Although surface buoyancy flux on the continental shelf appears as the major driver
 346 of ice-shelf basal melt changes, the set of curves in Fig. 8 do not exactly overlap, espe-
 347 cially the curve associated with the momentum flux perturbation. For a given buoyancy
 348 flux, the cold-climate momentum perturbation induces a slightly higher melt rate than

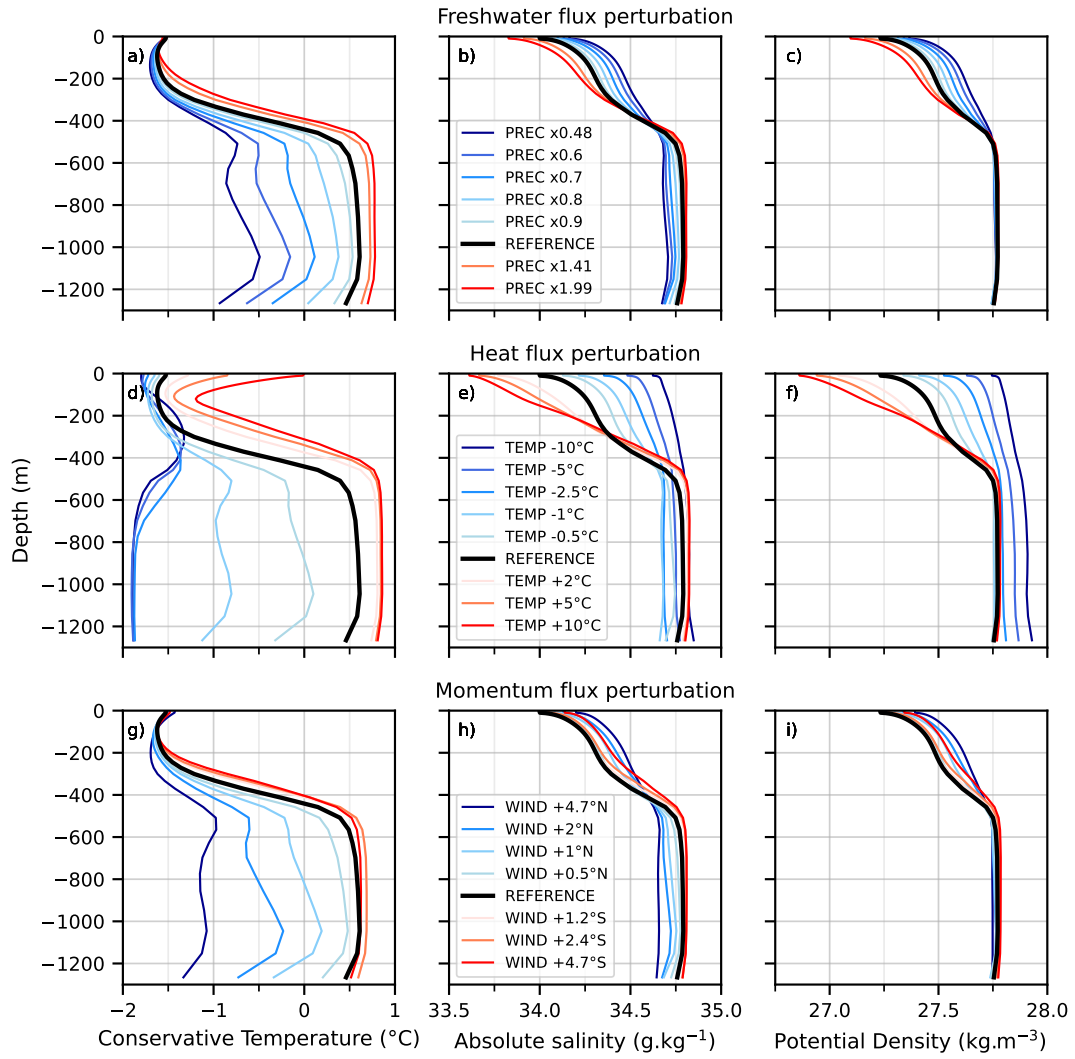


Figure 9. Shelf-averaged vertical profiles of conservative temperature (left), absolute salinity (middle) and potential density (right) over the period 1988-2018 for the various atmospheric perturbations : freshwater flux (top), heat flux (middle), and momentum flux (bottom) perturbations.

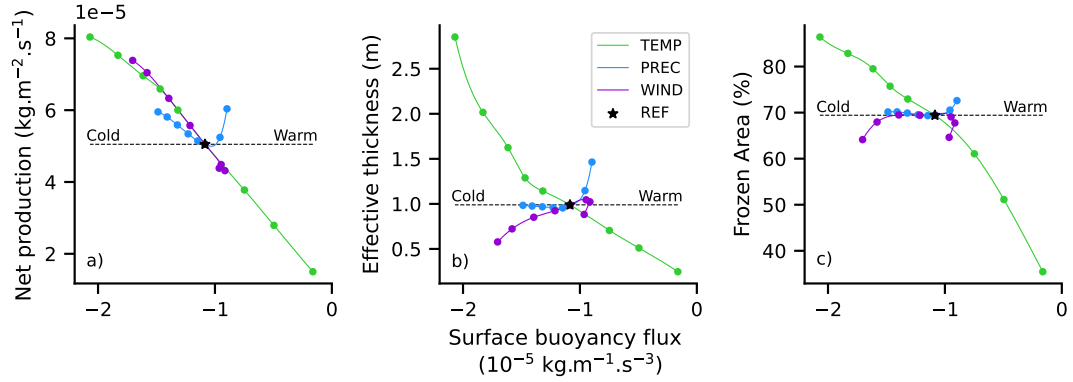


Figure 10. Sea-ice characteristics on the Amundsen Sea continental shelf related to surface buoyancy flux: (a) net production (i.e. growth minus melt), (b) effective thickness (mean thickness over the whole continental shelf including ice-free areas), and (c) frozen area. The star represents the reference case. The perturbed flux configurations are colored in green for heat, blue for freshwater, and purple for momentum.

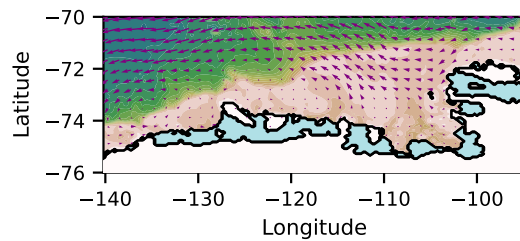


Figure 11. Sea-ice velocity anomaly relative to the reference case for a northward wind shift of 4.7°N . The background map is identical to the one shown in Fig. 1.

349 those related to freshwater and heat perturbations. The difference could be explained
 350 by Ekman dynamics if northward-shifted winds were associated with stronger Ekman
 351 upwelling, which would expose the ice shelves to a thicker layer of warm water (and, thus,
 352 partially inhibit the effects of decreased surface buoyancy fluxes). However, a stronger
 353 Ekman downwelling is found when considering the average velocity over the continen-
 354 tal shelf (Fig. 13a).

355 A more detailed analysis at the ice-shelf scale shows that these differences are only
 356 noticeable for the eastern ice shelves (Fig. 12), i.e., for Cosgrove, Pine Island and Thwaites,
 357 suggesting regional differences in the acting mechanisms. We, therefore, analyzed the Ek-
 358 man velocity at the entrance of the Pine Island–Thwaites Troughs as in Holland et al.
 359 (2019), but the most extreme point (+4.7°N) does not match either with the expected
 360 upwelling anomaly (Fig. 13b). Ekman pumping in our simulations is spatially very noisy
 361 (like Fig. 2a of Dotto et al., 2019), and we acknowledge a strong sensitivity to the ex-
 362 act location of the box used for the spatial average. Further investigation of Ekman ve-
 363 locities near individual ice-shelf fronts were similarly highly dependent on the location
 364 of box boundaries and therefore not conclusive. In summary, Ekman dynamics might
 365 explain the small difference in the melt response to the momentum perturbation and the
 366 other two perturbations, but such effect remains elusive. Other possible explanations may
 367 involve changes in ocean dynamics near the shelf break influencing the water mass prop-
 368 erties advected onto the continental shelf.

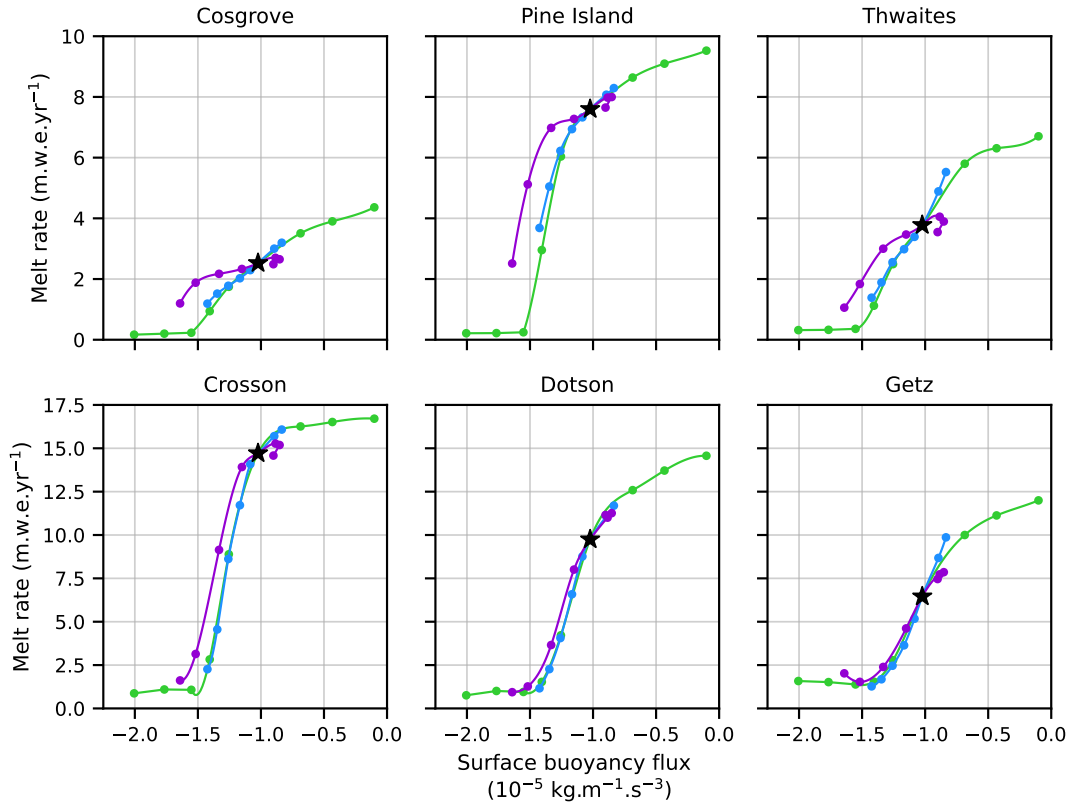


Figure 12. Mean basal melt rate of individual ice shelves in the Amundsen Sea as a function of the mean surface buoyancy flux over the Amundsen Sea continental shelf for the period 1988–2018. The green, blue and purple curves correspond to perturbations of heat, freshwater and momentum fluxes, respectively. The black star represents the reference case.

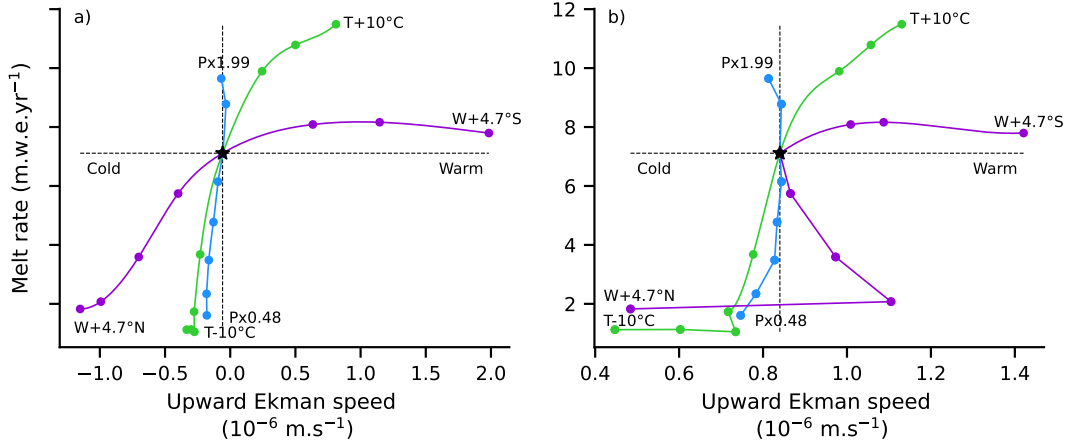


Figure 13. Mean basal melt rate as a function of upward Ekman velocity averaged over (a) the Amundsen Sea continental shelf and (b) over the entrance of Pine Island–Thwaites Troughs (box similar to the one defined in Fig. 1a of Holland et al. (2019)). The green, blue and purple curves correspond to perturbations of heat, freshwater and momentum fluxes, respectively. The black star represents the reference case.

369

4 Discussion and Conclusion

370

Robustness of the thresholds with respect to our model biases

371

372

373

374

375

376

377

378

379

380

381

382

383

384

385

386

387

Our regional model captures well the seasonal variability (see Section S3 in Supporting Information). Despite a calibration, however, the reference simulation still has a melt rate bias. The rate is outside the range of uncertainties of oceanic or satellite-based estimates, although of a similar order of magnitude to those found in other regional model studies (e.g., Nakayama et al., 2014; Kimura et al., 2017; Naughten et al., 2022), and has an overly low interannual variability (Figs. 4-5) compared to observational estimates (Dutrieux et al., 2014; Jenkins et al., 2018). Nevertheless, a more realistic interannual variability is observed for relatively small atmospheric perturbations. It should be kept in mind that a small perturbation of 0.5°C of the air temperature is of the order of magnitude of the reanalysis biases estimated by Jones et al. (2016) for the Amundsen Sea region. Biases are also large for precipitation, which is not constrained by data assimilation (Bromwich et al., 2011; Palerme et al., 2017). This means that the 'real' Amundsen Sea might correspond to a slightly cooler and drier climate than our reference state. However, the melt rate vs. buoyancy-flux curve is realistic and only the position of the reference state (black star) on this curve could be biased. Thus, the exact thresholds for air temperature, precipitation and wind shift for which a transition to the cold state occurs should still be considered as uncertain.

388

Robustness of the reversibility of abrupt transitions

389

390

391

392

393

394

395

396

Our results show that abrupt and reversible warm-to-cold as well as cold-to-warm transitions could occur in the Amundsen Sea for relatively weak regional atmospheric perturbations. The reversibility found in our experiments contrasts with the irreversibility of similar cold-to-warm transitions found in simulations of the Weddell Sea and Filchner-Ronne Ice-Shelf cavity (Hellmer et al., 2017; Hazel & Stewart, 2020; Comeau et al., 2022). The reason why the cold-to-warm transition is reversible in the Amundsen Sea but not in the Weddell Sea remains unclear. The melt-induced circulation was presented as the cause of the irreversibility in Hellmer et al. (2017), but the strong melt-induced circu-

397 lation in the Amundsen Sea after a cold-to-warm transition (Jourdain et al., 2017; Donat-
 398 Magnin et al., 2017) does not seem able to maintain the onshore flow of Circumpolar Deep
 399 Water when the forcing is reverted to cold climate conditions. For the coldest pertur-
 400 bations, the deep Amundsen Sea is approximately at a conservative temperature of -1.9°C
 401 and an absolute salinity of 34.7 g kg^{-1} (Fig. 9d,e), i.e., typical of the High Salinity Shelf
 402 Water (HSSW) produced in the Weddell Sea. Hazel and Stewart (2020) explains the Wed-
 403 dell Sea tipping point by a feedback of ice-shelf meltwater to the salinity of newly formed
 404 HSSW. The tipping conditions and associated hysteresis may, therefore, be sensitive to
 405 the ratio between the HSSW formation rate and total ice-shelf basal mass loss, which
 406 could explain different regimes in the Weddell and Amundsen Seas.

407 These transitions and their reversibility may be complicated or facilitated by ef-
 408 fects not taken into account in our simulations, such as the feedbacks with the large-scale
 409 atmospheric and oceanic circulations or the ice-sheet dynamics.

410 First of all, we do not change the ocean lateral boundary conditions in our sensi-
 411 tivity experiments, while the Amundsen Sea is also sensitive to changes of water prop-
 412 erties advected from remote locations (Nakayama et al., 2018). It is known that large
 413 atmospheric changes over multiple decades will have global effects, and we, therefore, ac-
 414 knowledge that our regional point of view is somewhat limited. Furthermore, strong mod-
 415 ifications of ice-shelf melting in the Amundsen Sea are expected to have significant con-
 416 sequences at circum-Antarctic (Nakayama et al., 2020) and global scales, with some pos-
 417 itive feedback in which more meltwater enhances the stratification and further exposes
 418 ice shelves to CDW (Merino et al., 2018; Bronselaer et al., 2018; Golledge et al., 2019).
 419 Such feedback is not considered in our study and it is difficult to estimate how they would
 420 affect the thresholds and reversibility of our transitions.

421 Another limitation of our study is the missing evolution of ice-sheet dynamics in
 422 response to changes in ice-shelf melting. In the presence of higher melt rates, ice shelves
 423 are expected to thin and their grounding line to retreat. Ice-shelf thinning may slow down
 424 melting, if the ice draft raises above the thermocline (De Rydt et al., 2014). Conversely,
 425 strong grounding line retreat may enhance melting by exposing a larger basal area to
 426 warm water and thus favoring a stronger melt-induced sub-ice shelf circulation (Donat-
 427 Magnin et al., 2017). For some geometrical configurations, the retreat of the calving front
 428 may also favor melting by facilitating the circulation into ice-shelf cavities (Bradley et
 429 al., 2022). If ice-shelf basal melt rates increase sufficiently, the ice dynamics is likely to
 430 cross tipping points (Rosier et al., 2021), which would irreversibly put the Amundsen
 431 Sea in a different state due to the aforementioned feedback. Nonetheless, it is difficult
 432 to quantify the exact thresholds for which irreversibility would be found without using
 433 a fully coupled ocean-ice-sheet model.

434 *Buoyancy vs wind-stress forcing*

435 There is a consensus that the intrusion of warm CDW on the continental shelf plays
 436 a major role in the variability of ice-shelf basal melting, but several different processes
 437 have been suggested to explain their transport. As several studies independently inves-
 438 tigate the eastern (Pine-Island-Thwaites) and western (Dotson-Getz) parts of the shelf
 439 (Wählin et al., 2012; Nakayama et al., 2013; Dotto et al., 2019) and as our study iden-
 440 tifies distinct regimes between these two parts, it seems suitable to separate the anal-
 441 ysis of processes according to these two regions.

442 Our study shows that the surface buoyancy flux on the shelf is the main driver of
 443 the multi-decadal changes in basal melting for the western Amundsen Sea (Dotson-Getz)
 444 regardless of perturbation. They also indicate no changes in local Ekman pumping in
 445 response to idealized wind perturbations, in contrast with the observational study by Kim
 446 et al. (2021), in which Ekman pumping along the Dotson-Getz trough explains 43% of
 447 the summer thermocline interannual variability. Dotto et al. (2020) have suggested that

448 local winds at the shelf break may affect the eastward undercurrent and thereby the heat
449 transport onto the continental shelf.

450 In the eastern Amundsen Sea (Cosgrove, Pine Island, Thwaites), our results again
451 indicate that changes in the surface buoyancy fluxes are the main drivers of ice-shelf melt
452 rate variations at multi-decadal time scales. A small deviation of the wind-perturbation
453 experiments (Fig. 8 - purple line) nonetheless suggests that other wind-related processes
454 might play a role, although the exact mechanism remains elusive. Previous studies have
455 largely attributed interannual variability of the eastern Amundsen Sea to Ekman pump-
456 ing at the shelf break (e.g., Holland et al., 2019; Dotto et al., 2019; Webber et al., 2019;
457 Naughten et al., 2022), although sea-ice formation can also play a role in some specific
458 years (St-Laurent et al., 2015; Webber et al., 2017).

459 In summary, changes in the surface buoyancy forcing appear to be the dominant
460 driver of the variations in ice-shelf melting in all our experiments, whereas most previ-
461 ous studies have emphasized the direct role of wind stress, in particular through Ekman
462 pumping. Part of the apparent discrepancy may be related to the multi-decadal time scale
463 of our perturbations, which can slowly induce a change in the baroclinic balances that
464 could overwhelm the relatively fast Ekman dynamics. We acknowledge, however, that
465 our wind perturbations are highly idealized and may not capture the full complexity of
466 wind changes at the continental shelf break, although we do have increasing Ekman ve-
467 locities at the shelf break for the transition from cold to warm climate.

468 *Implications for past and future climates*

469 Our results indicate cold Amundsen Sea cavities (close to surface freezing point)
470 for conditions of the Last Glacial Maximum (Fig. 8). This is consistent with grounding
471 lines of paleo-ice streams near the continental shelf break during the last glacial period
472 (Larter et al., 2014). Combined heat, freshwater and momentum perturbations main-
473 tained cold-cavities for climate conditions typical of -0.5°C compared to present day even
474 in the presence of CDW at the continental shelf break (red star in Fig. 8). This suggests
475 that pre-industrial conditions (approximately 1°C colder than present day (IPCC, 2021))
476 were associated with cold cavities in the Amundsen Sea. The transition to warm cav-
477 ities may have occurred or be occurring as multi-year oscillations between cold and warm
478 periods (Figs. 4-5). For conditions warmer than today, the decadal variability is relatively
479 weak and cavities remain permanently warm. Our idealized experiments suggest a grad-
480 ual but limited increase in ice-shelf basal melting in response to global warming beyond
481 present levels.

482 **Data and softwares**

483 The model version and set of parameters used to run our experiments are provided
484 in https://github.com/Astrolabe-JC/Simulations_NEMO. THE GITHUB REPOS-
485 ITORIES WILL BE ARCHIVED ON <http://zenodo.org> AFTER ACCEPTANCE.

486 **Acknowledgments**

487 The authors would like to acknowledge Clara Burgard for her valuable advice on figures
488 and presentations as well as H el ene Seroussi for her constructive feedback as a member
489 of the PhD committee.

490 This study was funded by the European Union’s Horizon 2020 research and inno-
491 vation programme under grant agreements No 820575 (TiPACCs) and by the French Na-
492 tional Research Agency under grant No ANR-19-CE01-0015 (EIS). This work was granted
493 access to the HPC resources of CINES under the allocation A0100106035 attributed by
494 GENCI.

References

495

496

497

498

499

500

501

502

503

504

505

506

507

508

509

510

511

512

513

514

515

516

517

518

519

520

521

522

523

524

525

526

527

528

529

530

531

532

533

534

535

536

537

538

539

540

541

542

543

544

545

546

547

548

549

- Bett, D. T., Holland, P. R., Naveira Garabato, A. C., Jenkins, A., Dutrieux, P., Kimura, S., & Fleming, A. (2020). The impact of the Amundsen Sea freshwater balance on ocean melting of the West Antarctic Ice Sheet. *Journal of Geophysical Research: Oceans*, *125*(9), e2020JC016305.
- Bradley, A. T., Bett, D. T., Dutrieux, P., De Rydt, J., & Holland, P. (2022). The influence of pine island ice shelf calving on melting.
- Bromwich, D. H., Nicolas, J. P., & Monaghan, A. J. (2011). An Assessment of Precipitation Changes over Antarctica and the Southern Ocean since 1989 in Contemporary Global Reanalyses. *Journal of Climate*, *24*(16), 4189.
- Bronselaer, B., Winton, M., Griffies, S. M., Hurlin, W. J., Rodgers, K. B., Sergienko, O. V., . . . Russell, J. L. (2018). Change in future climate due to Antarctic meltwater. *Nature*, *564*(7734). doi: 10.1038/s41586-018-0712-z
- Brovkin, V., Brook, E., Williams, J. W., Bathiany, S., Lenton, T. M., Barton, M., . . . Yu, Z. (2021). Past abrupt changes, tipping points and cascading impacts in the Earth system. *Nature Geoscience*, *14*(8). doi: 10.1038/s41561-021-00790-5
- Budge, J. S., & Long, D. G. (2018). A comprehensive database for Antarctic iceberg tracking using scatterometer data. *IEEE Journal of Selected Topics in Applied Earth Observations and Remote Sensing*, *11*(2), 434–442.
- Carrère, L., Lyard, F., Cancet, M., Guillot, A., & Roblou, L. (2012). FES2012: A new global tidal model taking advantage of nearly twenty years of altimetry. In *Proceedings of the 20 years of progress in radar altimetry symposium (venice, italy)* (pp. 1–20).
- Comeau, D., Asay-Davis, X. S., Begeman, C. B., Hoffman, M. J., Lin, W., Petersen, M. R., . . . others (2022). The DOE E3SM v1. 2 Cryosphere Configuration: Description and Simulated Antarctic Ice-Shelf Basal Melting. *Journal of Advances in Modeling Earth Systems*, *14*(2), e2021MS002468.
- Dekker, M. M., Von Der Heydt, A. S., & Dijkstra, H. A. (2018). Cascading transitions in the climate system. *Earth System Dynamics*, *9*(4). doi: 10.5194/esd-9-1243-2018
- De Rydt, J., Holland, P. R., Dutrieux, P., & Jenkins, A. (2014). Geometric and oceanographic controls on melting beneath Pine Island Glacier. *Journal of Geophysical Research: Oceans*, *119*(4), 2420–2438.
- Donat-Magnin, M., Jourdain, N. C., Kittel, C., Agosta, C., Amory, C., Gallée, H., . . . Chekki, M. (2021). Future surface mass balance and surface melt in the Amundsen sector of the West Antarctic Ice Sheet. *Cryosphere*, *15*(2). doi: 10.5194/tc-15-571-2021
- Donat-Magnin, M., Jourdain, N. C., Spence, P., Le Sommer, J., Gallée, H., & Durand, G. (2017). Ice-shelf melt response to changing winds and glacier dynamics in the amundsen sea sector, antarctica. *Journal of Geophysical Research: Oceans*, *122*(12), 10206–10224.
- Dotto, T. S., Garabato, A. C., Bacon, S., Holland, P. R., Kimura, S., Firing, Y. L., . . . Jenkins, A. (2019). Wind-driven processes controlling oceanic heat delivery to the amundsen sea, antarctica. *Journal of Physical Oceanography*, *49*(11). doi: 10.1175/JPO-D-19-0064.1
- Dotto, T. S., Naveira Garabato, A. C., Wåhlin, A. K., Bacon, S., Holland, P. R., Kimura, S., . . . Jenkins, A. (2020). Control of the Oceanic Heat Content of the Getz-Dotson Trough, Antarctica, by the Amundsen Sea Low. *Journal of Geophysical Research: Oceans*, *125*(8). doi: 10.1029/2020JC016113
- Dutrieux, P., De Rydt, J., Jenkins, A., Holland, P. R., Ha, H. K., Lee, S. H., . . . Schröder, M. (2014). Strong sensitivity of pine Island ice-shelf melting to climatic variability. *Science*, *343*(6167). doi: 10.1126/science.1244341
- Favier, L., Durand, G., Cornford, S. L., Gudmundsson, G. H., Gagliardini, O., Gillet-Chaulet, F., . . . Le Brocq, A. M. (2014). Retreat of Pine Island Glacier

- 550 controlled by marine ice-sheet instability. *Nature Climate Change*, 4(2). doi:
551 10.1038/nclimate2094
- 552 Garbe, J., Albrecht, T., Levermann, A., Donges, J. F., & Winkelmann, R. (2020).
553 The hysteresis of the Antarctic Ice Sheet. *Nature*, 585(7826). doi: 10.1038/
554 s41586-020-2727-5
- 555 Garcia, H., Boyer, T., Baranova, O., Locarnini, R., Mishonov, A., Grodsky, A., ...
556 Zweng, M. (2019). World Ocean Atlas 2018: Product Documentation.
- 557 Golledge, N. R., Keller, E. D., Gomez, N., Naughten, K. A., Bernales, J., Trusel,
558 L. D., & Edwards, T. L. (2019). Global environmental consequences of twenty-
559 first-century ice-sheet melt. *Nature*, 566(7742), 65–72.
- 560 Gray, W. R., de Lavergne, C., Wills, R. C., Menviel, L., Spence, P., Holzer, M., ...
561 Michel, E. (2021). Poleward shift in the southern hemisphere westerly winds
562 synchronous with the deglacial rise in co2.
- 563 Griffies, S. M., Biastoch, A., Böning, C., Bryan, F., Danabasoglu, G., Chassignet,
564 E. P., ... Yin, J. (2009). Coordinated Ocean-ice Reference Experiments
565 (COREs). *Ocean Modelling*, 26(1-2). doi: 10.1016/j.ocemod.2008.08.007
- 566 Gudmundsson, G. H. (2013). Ice-shelf buttressing and the stability of marine ice
567 sheets. *Cryosphere*, 7(2). doi: 10.5194/tc-7-647-2013
- 568 Hazel, J. E., & Stewart, A. L. (2020). Bistability of the Filchner-Ronne Ice Shelf
569 Cavity Circulation and Basal Melt. *Journal of Geophysical Research: Oceans*,
570 125(4), e2019JC015848.
- 571 Hellmer, H. H., Kauker, F., Timmermann, R., Determann, J., & Rae, J. (2012).
572 *Twenty-first-century warming of a large Antarctic ice-shelf cavity by a redi-*
573 *rected coastal current* (Vol. 485) (No. 7397). doi: 10.1038/nature11064
- 574 Hellmer, H. H., Kauker, F., Timmermann, R., & Hattermann, T. (2017). The fate
575 of the Southern Weddell sea continental shelf in a warming climate. *Journal of*
576 *Climate*, 30(12). doi: 10.1175/JCLI-D-16-0420.1
- 577 Hinkel, J., Church, J. A., Gregory, J. M., Lambert, E., Le Cozannet, G., Lowe,
578 J., ... van de Wal, R. (2019). Meeting User Needs for Sea Level Rise In-
579 formation: A Decision Analysis Perspective. *Earth's Future*, 7(3). doi:
580 10.1029/2018EF001071
- 581 Holland, P. R., Bracegirdle, T. J., Dutrieux, P., Jenkins, A., & Steig, E. J. (2019).
582 West Antarctic ice loss influenced by internal climate variability and anthro-
583 pogenic forcing. *Nature Geoscience*, 12(9). doi: 10.1038/s41561-019-0420-9
- 584 IPCC. (2021). Climate Change 2021. *The Physical Science Basis. Contribution of*
585 *Working Group 1 to Sixth Assessment Report of the Intergovernmental Panel*
586 *on Climate Change*.
- 587 Jacobs, S., Hellmer, H. H., & Jenkins, A. (1996). Antarctic ice sheet melting in the
588 southeast pacific. *Geophysical Research Letters*, 23(9), 957–960.
- 589 Jacobs, S., Jenkins, A., Hellmer, H., Giulivi, C., Nitsche, F., Huber, B., & Guerrero,
590 R. (2012). The Amundsen Sea and the Antarctic ice sheet. *Oceanography*,
591 25(3). doi: 10.5670/oceanog.2012.90
- 592 Jenkins, A., Shoosmith, D., Dutrieux, P., Jacobs, S., Kim, T. W., Lee, S. H., ...
593 Stammerjohn, S. (2018). West Antarctic Ice Sheet retreat in the Amundsen
594 Sea driven by decadal oceanic variability. *Nature Geoscience*, 11(10). doi:
595 10.1038/s41561-018-0207-4
- 596 Jones, R. W., Renfrew, I. A., Orr, A., Webber, B. G., Holland, D. M., & Lazzara,
597 M. A. (2016). Evaluation of four global reanalysis products using in situ ob-
598 servations in the amundsen sea embayment, antarctica. *Journal of Geophysical*
599 *Research*, 121(11). doi: 10.1002/2015JD024680
- 600 Joughin, I., Smith, B. E., & Medley, B. (2014). Marine ice sheet collapse potentially
601 under way for the thwaites glacier basin, West Antarctica. *Science*, 344(6185).
602 doi: 10.1126/science.1249055
- 603 Jourdain, N. C., Mathiot, P., Merino, N., Durand, G., Le Sommer, J., Spence, P., ...
604 Madec, G. (2017). Ocean circulation and sea-ice thinning induced by melting

- ice shelves in the Amundsen Sea. *Journal of Geophysical Research: Oceans*, 122(3). doi: 10.1002/2016JC012509
- 605
606 Jourdain, N. C., Molines, J. M., Le Sommer, J., Mathiot, P., Chanut, J., de
607 Lavergne, C., & Madec, G. (2019). Simulating or prescribing the influ-
608 ence of tides on the Amundsen Sea ice shelves. *Ocean Modelling*, 133. doi:
609 10.1016/j.ocemod.2018.11.001
610
- 611 Kim, T. W., Yang, H. W., Dutrieux, P., Wåhlin, A. K., Jenkins, A., Kim, Y. G., ...
612 Cho, Y. K. (2021). Interannual Variation of Modified Circumpolar Deep Water
613 in the Dotson-Getz Trough, West Antarctica. *Journal of Geophysical Research:
614 Oceans*, 126(12). doi: 10.1029/2021JC017491
- 615 Kimura, S., Jenkins, A., Regan, H., Holland, P. R., Assmann, K. M., Whitt, D. B.,
616 ... Dutrieux, P. (2017). Oceanographic controls on the variability of ice-
617 shelf basal melting and circulation of glacial meltwater in the Amundsen Sea
618 Embayment, Antarctica. *Journal of Geophysical Research: Oceans*, 122(12),
619 10131–10155.
- 620 Large, W. G., & Yeager, S. G. (2004). *Diurnal to decadal global forcing for ocean
621 and sea-ice models: The data sets and flux climatologies*. Citeseer.
- 622 Larter, R. D., Anderson, J. B., Graham, A. G., Gohl, K., Hillenbrand, C. D., Jakob-
623 sson, M., ... Spiegel, C. (2014). *Reconstruction of changes in the Amundsen
624 Sea and Bellingshausen Sea sector of the West Antarctic Ice Sheet since the
625 Last Glacial Maximum* (Vol. 100). doi: 10.1016/j.quascirev.2013.10.016
- 626 Lee, J.-Y., Marotzke, J., Bala, G., Cao, L., Corti, S., Dunne, J. P., ... others (2021).
627 Future global climate: scenario-based projections and near-term information.
628 IPCC.
- 629 Ligtenberg, S. R., van de Berg, W. J., van den Broeke, M. R., Rae, J. G., & van
630 Meijgaard, E. (2013). Future surface mass balance of the Antarctic ice sheet
631 and its influence on sea level change, simulated by a regional atmospheric
632 climate model. *Climate Dynamics*, 41(3-4). doi: 10.1007/s00382-013-1749-1
- 633 Lindsey, A. A. (1995). The exploration history of the Lindsey Islands, Antarctica,
634 1928-1994. In *Proceedings of the Indiana Academy of Science* (Vol. 104, pp. 85–
635 92).
- 636 Lyard, F., Lefevre, F., Letellier, T., & Francis, O. (2006). Modelling the global
637 ocean tides: modern insights from fes2004. *Ocean dynamics*, 56(5-6), 394–415.
- 638 Madec, G., & the NEMO Team. (2016). NEMO ocean engine. *Note du Pôle de
639 modélisation*(27).
- 640 Marshall, J., & Plumb, R. A. (2008). *Atmosphere, Ocean, and Climate Dynamics*.
- 641 Masson-Delmotte, V., Stenni, B., Pol, K., Braconnot, P., Cattani, O., Falourd,
642 S., ... Otto-Bliesner, B. (2010). EPICA Dome C record of glacial
643 and interglacial intensities. *Quaternary Science Reviews*, 29(1-2). doi:
644 10.1016/j.quascirev.2009.09.030
- 645 Mathiot, P., Jenkins, A., Harris, C., & Madec, G. (2017). Explicit representa-
646 tion and parametrised impacts of under ice shelf seas in the z^* - coordinate
647 ocean model NEMO 3.6. *Geoscientific Model Development*, 10(7). doi:
648 10.5194/gmd-10-2849-2017
- 649 Matsuoka, K., Skoglund, A., Roth, G., de Pomereu, J., Griffiths, H., Headland, R.,
650 ... Melvær, Y. (2021). Quantarctica, an integrated mapping environment for
651 Antarctica, the Southern Ocean, and sub-Antarctic islands. *Environmental
652 Modelling and Software*, 140. doi: 10.1016/j.envsoft.2021.105015
- 653 Mazur, A., Wåhlin, A. K., & Krezel, A. (2017). An object-based SAR image iceberg
654 detection algorithm applied to the Amundsen Sea. *Remote Sensing of Environ-
655 ment*, 189, 67–83.
- 656 Merino, N., Jourdain, N. C., Le Sommer, J., Goosse, H., Mathiot, P., & Durand, G.
657 (2018). Impact of increasing Antarctic glacial freshwater release on regional
658 sea-ice cover in the Southern Ocean. *Ocean Modelling*, 121, 76–89.
- 659 Merino, N., Le Sommer, J., Durand, G., Jourdain, N. C., Madec, G., Mathiot, P.,

- 660 & Tournadre, J. (2016). Antarctic icebergs melt over the Southern Ocean :
 661 Climatology and impact on sea ice. , *104*. doi: 10.1016/j.ocemod.2016.05.001
- 662 Morlighem, M., Rignot, E., Binder, T., Blankenship, D., Drews, R., Eagles, G., ...
 663 Young, D. A. (2020). Deep glacial troughs and stabilizing ridges unveiled
 664 beneath the margins of the Antarctic ice sheet. *Nature Geoscience*, *13*(2). doi:
 665 10.1038/s41561-019-0510-8
- 666 Nakayama, Y., Menemenlis, D., Zhang, H., Schodlok, M., & Rignot, E. (2018).
 667 Origin of Circumpolar Deep Water intruding onto the Amundsen and Belling-
 668 shausen Sea continental shelves. *Nature Communications*, *9*(1). doi:
 669 10.1038/s41467-018-05813-1
- 670 Nakayama, Y., Schröder, M., & Hellmer, H. H. (2013). From circumpolar deep water
 671 to the glacial meltwater plume on the eastern amundsen shelf. *Deep Sea Re-*
 672 *search Part I: Oceanographic Research Papers*, *77*, 50–62.
- 673 Nakayama, Y., Timmermann, R., & Hellmer, H. (2020). Impact of west antarctic
 674 ice shelf melting on southern ocean hydrography. *The Cryosphere*, *14*(7),
 675 2205–2216.
- 676 Nakayama, Y., Timmermann, R., Schröder, M., & Hellmer, H. H. (2014). On
 677 the difficulty of modeling Circumpolar Deep Water intrusions onto the
 678 Amundsen Sea continental shelf. *Ocean Modelling*, *84*. doi: 10.1016/
 679 j.ocemod.2014.09.007
- 680 Naughten, K. A., Holland, P. R., Dutrieux, P., Kimura, S., Bett, D. T., & Jenkins,
 681 A. (2022). Simulated twentieth-century ocean warming in the amundsen sea,
 682 west antarctica. *Geophysical Research Letters*, e2021GL094566.
- 683 Palerme, C., Claud, C., Dufour, A., Genthon, C., Wood, N. B., & L'Ecuyer, T.
 684 (2017). Evaluation of Antarctic snowfall in global meteorological reanalyses.
 685 *Atmospheric Research*, *190*, 104–112.
- 686 Pattyn, F., Schoof, C., Perichon, L., Hindmarsh, R. C., Bueler, E., De Fleurian, B.,
 687 ... Vieli, A. (2012). Results of the marine ice sheet model intercomparison
 688 project, MISIMP. *Cryosphere*, *6*(3). doi: 10.5194/tc-6-573-2012
- 689 Rignot, E., Jacobs, S., Mouginot, J., & Scheuchl, B. (2013). Ice-shelf melting around
 690 antarctica. *Science*, *341*(6143). doi: 10.1126/science.1235798
- 691 Rosier, S. H., Reese, R., Donges, J. F., De Rydt, J., Hilmar Gudmundsson, G.,
 692 & Winkelmann, R. (2021). The tipping points and early warning indi-
 693 cators for Pine Island Glacier, West Antarctica. *Cryosphere*, *15*(3). doi:
 694 10.5194/tc-15-1501-2021
- 695 Rousset, C., Vancoppenolle, M., Madec, G., Fichefet, T., Flavoni, S., Barthélemy,
 696 A., ... Vivier, F. (2015). The Louvain-La-Neuve sea ice model LIM3.6:
 697 Global and regional capabilities. *Geoscientific Model Development*, *8*(10). doi:
 698 10.5194/gmd-8-2991-2015
- 699 Schoof, C. (2007). Marine ice-sheet dynamics. Part 1. The case of rapid sliding.
 700 *Journal of Fluid Mechanics*, *573*. doi: 10.1017/S0022112006003570
- 701 Smith, J. A., Andersen, T. J., Shortt, M., Gaffney, A. M., Truffer, M., Stanton,
 702 T. P., ... Vaughan, D. G. (2017). Sub-ice-shelf sediments record history of
 703 twentieth-century retreat of Pine Island Glacier. *Nature*, *541*(7635). doi:
 704 10.1038/nature20136
- 705 Spence, P., Griffies, S. M., England, M. H., Hogg, A. M. C., Saenko, O. A., & Jour-
 706 dain, N. C. (2014). Rapid subsurface warming and circulation changes of
 707 Antarctic coastal waters by poleward shifting winds. *Geophysical Research*
 708 *Letters*, *41*(13). doi: 10.1002/2014GL060613
- 709 St-Laurent, P., Klinck, J., & Dinniman, M. (2015). Impact of local winter cooling
 710 on the melt of Pine Island Glacier, Antarctica. *Journal of Geophysical Re-*
 711 *search: Oceans*, *120*(10), 6718–6732.
- 712 Talley, L. D., Pickard, G. L., Emery, W. J., & Swift, J. H. (2011). *Descriptive phys-*
 713 *ical oceanography: An introduction: Sixth edition*. doi: 10.1016/C2009-0-24322
- 714 -4

- 715 Tsujino, H., Urakawa, S., Nakano, H., Small, R. J., Kim, W. M., Yeager, S. G., ...
716 others (2018). JRA-55 based surface dataset for driving ocean–sea-ice models
717 (JRA55-do). *Ocean Modelling*, *130*, 79–139.
- 718 Turney, C. S., Fogwill, C. J., Golledge, N. R., McKay, N. P., van Sebille, E., Jones,
719 R. T., ... others (2020). Early last interglacial ocean warming drove sub-
720 stantial ice mass loss from antarctica. *Proceedings of the National Academy of*
721 *Sciences*, *117*(8), 3996–4006.
- 722 Wählin, A. K., Muench, R. D., Arneborg, L., Björk, G., Ha, H. K., Lee, S. H., &
723 Alsén, H. (2012). Some implications of ekman layer dynamics for cross-shelf
724 exchange in the Amundsen sea. *Journal of Physical Oceanography*, *42*(9). doi:
725 10.1175/JPO-D-11-041.1
- 726 Webber, B. G., Heywood, K. J., Stevens, D. P., & Assmann, K. M. (2019). The
727 impact of overturning and horizontal circulation in pine Island trough on ice
728 shelf melt in the eastern Amundsen Sea. *Journal of Physical Oceanography*,
729 *49*(1). doi: 10.1175/JPO-D-17-0213.1
- 730 Webber, B. G., Heywood, K. J., Stevens, D. P., Dutrieux, P., Abrahamsen, E. P.,
731 Jenkins, A., ... Kim, T. W. (2017). Mechanisms driving variability in
732 the ocean forcing of Pine Island Glacier. *Nature Communications*, *8*. doi:
733 10.1038/ncomms14507
- 734 Wunderling, N., Donges, J. F., Kurths, J., & Winkelmann, R. (2021). Interacting
735 tipping elements increase risk of climate domino effects under global warming.
736 *Earth System Dynamics*, *12*(2). doi: 10.5194/esd-12-601-2021